ISSN 1674-1056
http://cpb.iphy.ac.cn
http://iopscience.iop.org/cpb
中国物理 B
Chinese Physics
中国物理
Chinese Physics B

Band engineering and precipitation enhance thermoelectric performance of SnTe with Zn-doping

Zhiyu Chen(陈志禹), Ruifeng Wang(王瑞峰), Guoyu Wang(王国玉), Xiaoyuan Zhou(周小元), Zhengshang Wang(王正上), Cong Yin(尹聪), Qing Hu(胡庆), Binqiang Zhou(周斌强), Jun Tang(唐军), Ran Ang(昂然)
Citation: Chin. Phys. B . 2018, 27(4): 047202. **doi:** 10.1088/1674-1056/27/4/047202

Journal homepage: http://cpb.iphy.ac.cn; http://iopscience.iop.org/cpb

What follows is a list of articles you may be interested in

Ultrafast interlayer photocarrier transfer in graphene-$MoSe_2$ van der Waals heterostructure

Xin-Wu Zhang(张心悟), Da-Wei He(何大伟), Jia-Qi He(何佳琪), Si-Qi Zhao(赵思淇), Sheng-Cai Hao(郝生财), Yong-Sheng Wang(王永生), Li-Xin Yi(衣立新)
Chin. Phys. B . 2017, 26(9): 097202. **doi:** 10.1088/1674-1056/26/9/097202

Improved thermoelectric performance in p-type $Bi_{0.48}Sb_{1.52}Te_3$ bulk material by adding $MnSb_2Se_4$

Binglei Cao(曹丙垒), Jikang Jian(简基康), Binghui Ge(葛炳辉), Shanming Li(李善明), Hao Wang(王浩), Jiao Liu(刘骄), Huaizhou Zhao(赵怀周)
Chin. Phys. B . 2017, 26(1): 017202. **doi:** 10.1088/1674-1056/26/1/017202

Band gap anomaly and topological properties in lead chalcogenides

Simin Nie(聂思敏), Xiao Yan Xu(许霄琰), Gang Xu(徐刚), Zhong Fang(方忠)
Chin. Phys. B . 2016, 25(3): 037311. **doi:** 10.1088/1674-1056/25/3/037311

Au and Ti induced charge redistributions on monolayer WS_2

Zhu Hui-Li, Yang Wei-Huang, Wu Ya-Ping, Lin Wei, Kang Jun-Yong, Zhou Chang-Jie
Chin. Phys. B . 2015, 24(7): 077301. **doi:** 10.1088/1674-1056/24/7/077301

SPECIAL TOPIC — Recent advances in thermoelectric materials and devices

Band engineering and precipitation enhance thermoelectric performance of SnTe with Zn-doping*

Zhiyu Chen(陈志禹)[1], Ruifeng Wang(王瑞峰)[2,3], Guoyu Wang(王国玉)[2,3], Xiaoyuan Zhou(周小元)[4], Zhengshang Wang(王正上)[1], Cong Yin(尹聪)[1], Qing Hu(胡庆)[1], Binqiang Zhou(周斌强)[5], Jun Tang(唐军)[1,6,‡], and Ran Ang(昂然)[1,6,†]

[1] *Key Laboratory of Radiation Physics and Technology, Ministry of Education, Institute of Nuclear Science and Technology, Sichuan University, Chengdu* 610064, *China*

[2] *Chongqing Institute of Green and Intelligent Technology, Chinese Academy of Sciences, Chongqing* 400714, *China*

[3] *University of Chinese Academy of Sciences, Beijing* 100190, *China*

[4] *College of Physics, Chongqing University, Chongqing* 401331, *China*

[5] *School of Materials Science and Engineering, Tongji University, Shanghai* 201804, *China*

[6] *Institute of New Energy and Low-Carbon Technology, Sichuan University, Chengdu* 610065, *China*

(Received 19 December 2017; revised manuscript received 9 January 2018; published online 10 March 2018)

We have systematically studied the thermoelectric properties in Zn-doped SnTe. Strikingly, band convergence and embedded precipitates arising from Zn doping, can trigger a prominent improvement of thermoelectric performance. In particular, the value of dimensionless figure of merit zT has increased by 100% and up to ~ 0.5 at 775 K for the optimal sample with 2% Zn content. Present findings demonstrate that carrier concentration and effective mass play crucial roles on the Seebeck coefficient and power factor. The obvious deviation from the Pisarenko line (Seebeck coefficient versus carrier concentration) due to Zn-doping reveals the convergence of valence bands. When the doping concentration exceeds the solubility, precipitates occur and lead to a reduction of lattice thermal conductivity. In addition, bipolar conduction is suppressed, indicating an enlargement of band gap. The Zn-doped SnTe is shown to be a promising candidate for thermoelectric applications.

Keywords: thermoelectric materials, chalcogenide, band engineering, precipitation

PACS: 72.15.Jf, 73.50.Lw, 74.25.F–, 74.25.fg **DOI:** 10.1088/1674-1056/27/4/047202

1. Introduction

Thermoelectric energy conversion technology has successfully been applied in deep-space exploration for an electrical power supply,[1] and is now attracting extensive attention to resolve the energy and environmental issues.[2] Therefore, it is significant to develop efficient thermoelectric materials or devices, which can utilize waste heat in direct conversion. From the viewpoint of promising applications, thermoelectric materials with high dimensionless figure of merit (zT) include clathrates,[3,4] Zintl phase,[5,6] half-Heusler,[7,8] filled skutterudites,[9,10] chalcogenides,[11–13] etc. Particularly, SnTe, as a typical representative in chalcogenides,[14–16] is characterized by a two-valence-band structure.[17] To some extent, such a band structure is beneficial to decouple the correlation among Seebeck coefficient S, electrical conductivity σ, and thermal conductivity κ.[14] However, the large energy offset $\Delta E_{\mathrm{L}-\Sigma}$ between upper light hole band (L band) and second lower-lying heavy hole band (Σ band),[18] and relative higher lattice thermal conductivity κ_{l} restrict the improvement of thermoelectric performance in SnTe.[19] In general, chemical doping of SnTe is an effective approach to enhance zT.[20–26] Especially for Cd- and Hg-doping,[21,26] which can effectively modulate the band structure of SnTe, thus enhancing zT. Taking into account the fact that Zn is the family element of Cd and Hg, the Zn-doping should also have an analogous effect. Recently, the first-principles calculation on Zn-doped SnTe indicate that Zn-doping converge the two valence bands, and distinctly reinforce S and σ.[27] Unfortunately, the experimental study on Zn-doped SnTe does not exhibit this.[28] Moreover, the underlying thermoelectric properties have not been clarified. Indisputably, it is urgent to systematically investigate the intrinsic thermoelectric feature of Zn-doped SnTe.

In this study, we provide direct evidences that Zn-doping in SnTe induces a noticeable enhancement of thermoelectric performance due to band convergence[29] and precipitation. It is worth noting that the value of zT for the optimal sample with a 2% Zn content has improved by 100% and reaches ~ 0.5

*Project supported by the National Natural Science Foundation of China (Grant No. 51771126), the Youth Foundation of Science & Technology Department of Sichuan Province, China (Grant No. 2016JQ0051), the Sichuan University Talent Introduction Research Funding (Grand No. YJ201537), the Sichuan University Outstanding Young Scholars Research Funding (Grant No. 2015SCU04A20), the World First-Class University Construction Funding, and the Fundamental and Frontier Research in Chongqing (Grant No. CSTC2015JCYJBX0026).

†Corresponding author. E-mail: rang@scu.edu.cn

‡Corresponding author. E-mail: tangjun@scu.edu.cn

© 2018 Chinese Physical Society and IOP Publishing Ltd

at 775 K. Combining the Hall measurement, we demonstrate that carrier concentration and effective mass dominate S and the power factor. The values of S increase in Zn-doped SnTe owing to the reduction of energy offset $\Delta E_{L-\Sigma}$ between L band and Σ band. Furthermore, the strengthened phonon scattering due to precipitates, effectively decreases the lattice thermal conductivity κ_l. Additionally, the observed weaker bipolar conduction reveals the broadening band gap. It is therefore reasonable to conclude that Zn-doped SnTe shows a great potential for thermoelectric applications.

2. Experimental procedure

Polycrystalline $Sn_{1-x}Zn_xTe$ ($x = 0, 0.01, 0.02, 0.04$) samples were synthesized by the conventional solid-state reaction method. Stoichiometric quantities of high purity elements ($> 99.99\%$) were loaded into quartz tubes that were evacuated, flame-sealed, slowly heated to 1123 K, soaked at this temperature for 24 h and then subsequently quenched by water. The obtained ingot was crushed into powders and densified at 823 K under 60 MPa for 3 min by spark plasma sintering (SPS). All the disk-shaped samples obtained were 10 mm in diameter with density no less than 95% of theoretical density (6.46 g·cm^{-3}). Powder x-ray diffraction (XRD) was carried out on a DX-2700 x-ray diffractometer using Cu Kα radiation. Structural refinements were performed by using Rietveld analysis. The composition and microstructure are determined by energy dispersive spectroscopy (EDS) and scanning electron microscopy (SEM). The temperature dependence of electrical conductivity σ and Seebeck coefficient S were carried out by using apparatus (LSR-3). The temperature dependence of thermal diffusivity and thermal conductivity κ were performed by the laser flash method (LFA 457, Netzsch). The Hall coefficient R_H and carrier concentration n were determined by using the Van der Pauw technique.

3. Experimental results and discussion

The powder XRD patterns of $Sn_{1-x}Zn_xTe$ ($x = 0$, 0.01, 0.02, 0.04) are shown in Fig. 1(a). The main Bragg reflections of all samples confirm the rock-salt structure (space group $Fm\bar{3}m$) as plotted in the inset of Fig. 1(a). Within the detection limit, no impurity phases were observed for $x \leq 0.02$. However, with x increasing to $x = 0.04$, the peaks of the second phase arise ($2\theta = 25.2°$, 41.9°), which match with the powder XRD pattern of ZnTe. It is noted that the peak shifts of XRD are not very obvious due to the minor doping. It needs to utilize Rietveld refinement to obtain the variation of lattice parameters. Figure 1(b) shows the powder XRD and structural Rietveld refinement for $x = 0.02$. The refined lattice parameter a of all samples are displayed in Fig. 1(c). The refinement error is ~ 0.0003 Å. Apparently, the value of a monotonously decreases with increasing Zn content, in accordance with the reduction of ironic radius from Sn^{2+} to Zn^{2+}. Interestingly, the variation of a follows the Vegard law well for $x \leq 0.02$, while it obviously deviates from this law for $x = 0.04$, revealing that the solid solubility of Zn in SnTe is about 2%. To probe the microstructure of $x = 0.04$, we carried out the SEM characterization. It is clearly seen that numerous precipitates exist (bright white region) embedded in the matrix (dark black region) as shown in Fig. 1(d). To determine the element distribution of precipitates, we performed the EDS analysis deriving from spots 1 and 2 in Fig. 1(e). The EDS results demonstrate Zn, Sn, and Te distribution, pointing to the chemical composition of precipitates which are rich in Zn (spot 1) while the compositions of the matrix are deficient in Zn (spot 2) as plotted in Fig. 1(f).

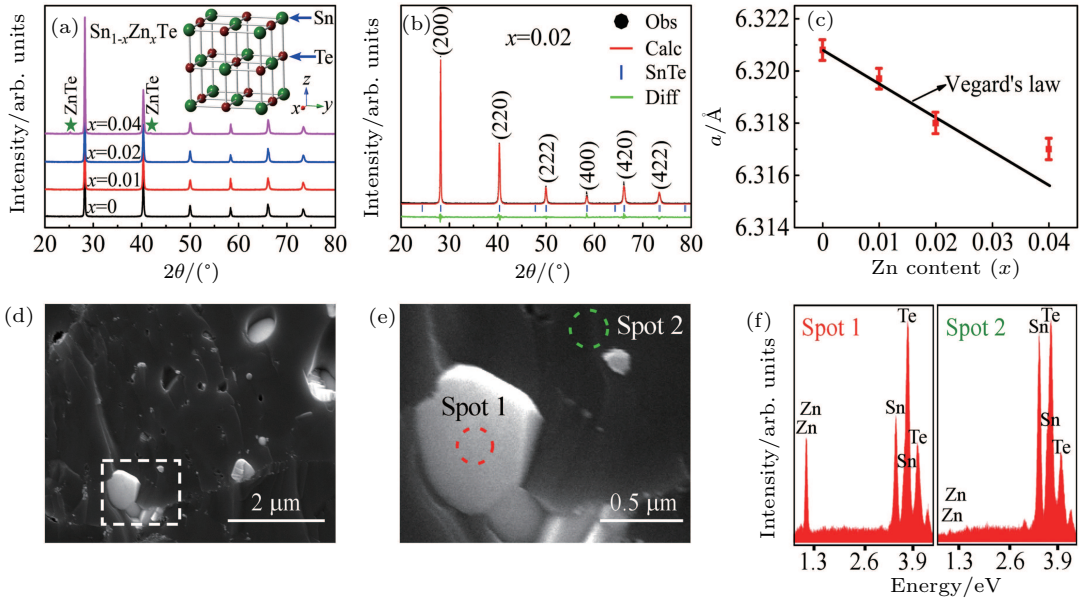


Fig. 1. (color online) (a) Powder XRD patterns for $Sn_{1-x}Zn_xTe$ ($x = 0$, 0.01, 0.02, 0.04) at room temperature. Inset: Crystal structure of SnTe. (b) Powder XRD pattern with Rietveld refinement for the sample with $x = 0.02$. (c) Lattice parameter a as a function of Zn content x. The solid line represents Vegard's law. (d) SEM image for the sample with $x = 0.04$. (e) Magnified SEM image within the white square area in panels (d). (f) The corresponding EDS results for spot 1 and spot 2 in image (e), respectively.

Understanding the origin of the improvement of S is of extreme significance for rationally designing high-performance thermoelectric materials. The character of S can be approximated by $S = (8\pi^2 k_B^2/3eh^2)m^*T(\pi/3n)^{2/3}$ in the degenerate case, where n is the carrier concentration, and m^* is the effective mass of the carrier.[26] It is surprising that Zn, although nominally isovalent with Sn, actually emerges to serve as an electron donor. The reason could be the reduction of Sn vacancies caused by Zn substitution, giving rise to the decrease of hole concentration n until $x = 0.02$, as plotted in Fig. 2(c). Nevertheless, excessive Zn-driven precipitates increase n for $x = 0.04$. As to effective mass m^*, the values of m^* for all Zn-doped samples rise. Especially for $x = 0.01$, m^* reaches the largest value $\sim 0.2m_e$, where m_e is the bare electron mass.

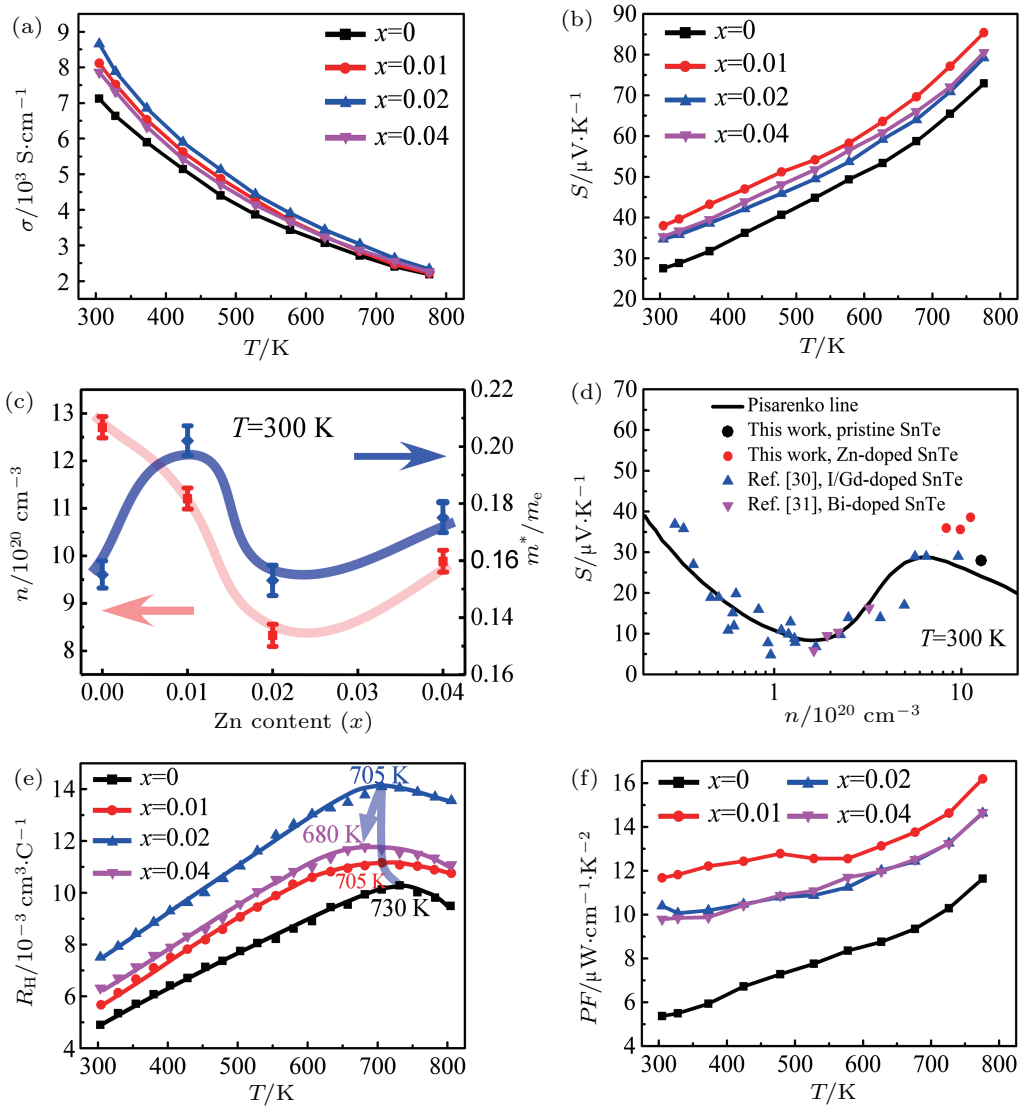


Fig. 2. (color online) Temperature-dependent (a) electrical conductivity σ and (b) Seebeck coefficient S for all samples. (c) Carrier concentration n and effective mass m^* at room temperature as a function of Zn content x. (d) Room temperature Pisarenko plot, in comparison with reported data from Refs. [30] and [31]. The solid line is based on a two-band model.[30] (e) Temperature-dependent Hall coefficient R_H and (f) power factor PF.

To gain more insights into the correlation between Seebeck coefficient S and hole concentration n, we performed the well-established Pisarenko plot obtained from a two-band model.[30] As plotted in Fig. 3(d), the data points for pristine SnTe in this work, combined with previous reported I/Gd- and Bi-doped SnTe,[30,31] follows the Pisarenko line well. However, the values of S for Zn-doped samples are higher than the theoretical prediction, which can be attributed to the valence band convergence induced by Zn-doping. To obtain more evidence for the band convergence, we probe the temperature-dependent Hall coefficient R_H as shown in Fig. 2(e). With increasing the temperature, R_H increases due to the band offset $\Delta E_{L-\Sigma}$ and the redistribution of carriers between L band and Σ band. The peak of R_H, which is the feature of band convergence,[24] shifts towards low temperature from ~ 730 K ($x = 0$) to ~ 680 K ($x = 0.04$). Such a decreased temperature of peak R_H indicates the reduction of $\Delta E_{L-\Sigma}$. The power factor (PF) displays a large enhancement for Zn-doped samples [see Fig. 2(f)], which is determined by hole concentration n and effective mass m^*.

The temperature dependence of total thermal conductivity κ is shown in Fig. 3(a). κ can be expressed by the sum of lattice component κ_l and mobile electronic component κ_e as $\kappa = \kappa_l + \kappa_e$. The value of κ_e can be estimated from Wiedemann–Franz law, $\kappa_e = L\sigma T$ (L is the Lorenz number estimated by a single Kane band model[25]). The value of κ_l was calculated and plotted in Fig. 3(b). For pristine and Zn-doped samples, κ_l decreases with increasing the temperature due to phonon–phonon Umklapp scattering and then increases at elevated temperatures because of the bipolar effect. It is expected that the Umklapp scattering dominate phonon scattering above Debye temperature. Namely, κ_l is linearly proportional to $1/T$. The plot of κ_l as a function of $1/T$ is present in Fig. 3(c). For $x = 0$, κ_l starts to deviate from the linear relationship as the temperature increases to ~ 630 K, revealing the contribution of bipolar diffusion κ_{bip}. The κ_{bip} at 775 K as a function of x is illustrated in the inset of Fig. 3(c). It is noted that the contribution of κ_{bip} gradually decreases from 0.22 $W\cdot m^{-1}\cdot K^{-1}$ for $x = 0$ to 0.12 $W\cdot m^{-1}\cdot K^{-1}$ for $x = 0.04$. Usually, a high hole concentration n and large band gap E_g are beneficial to suppress bipolar diffusion. The decrease of κ_{bip} demonstrates the widened band gap due to Zn-doping, even as hole concentration reduces in this case.

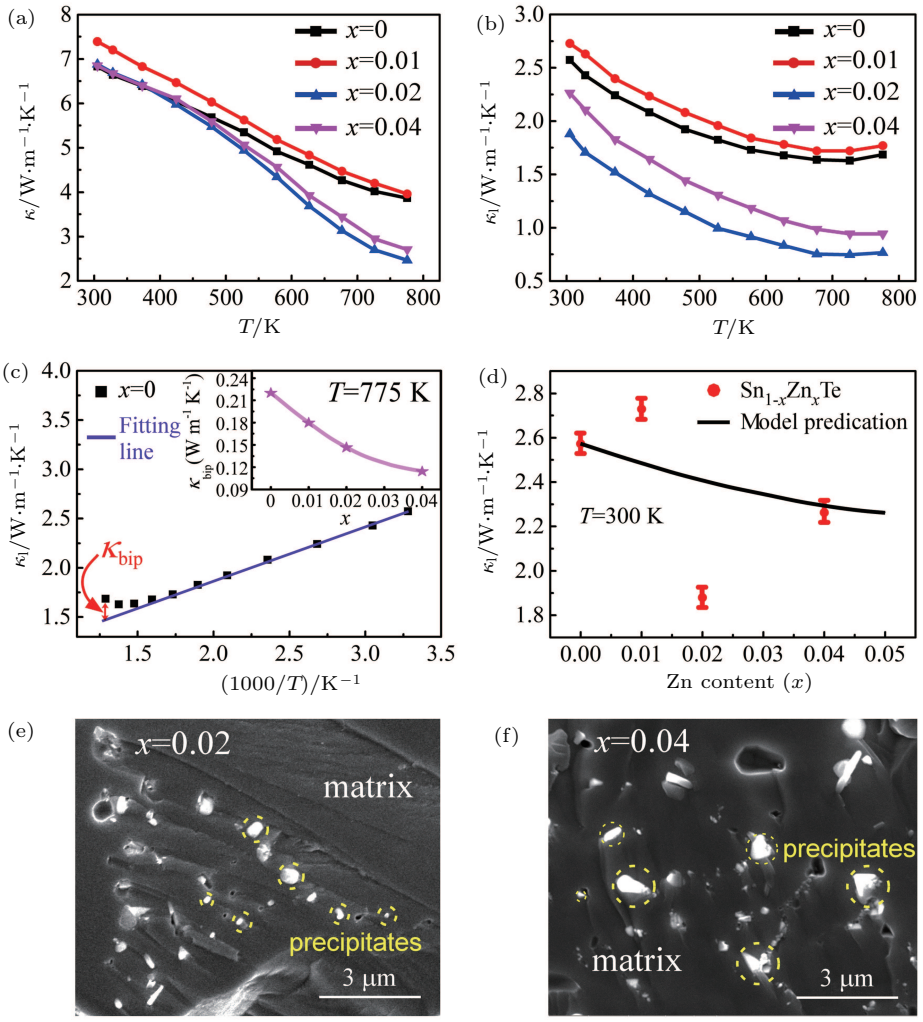


Fig. 3. (color online) Temperature-dependent (a) total thermal conductivity κ and (b) lattice thermal conductivity κ_l for all samples. (c) The κ_l as a function of $1000/T$ for pristine SnTe. The solid line represents linear fitting, and deviation of thermal conductivity indicates the contribution of bipolar diffusion κ_{bip}. Inset: the κ_{bip} as a function of Zn content x. (d) Room temperature κ_l as a function of x. The solid line corresponds to the prediction of κ_l according to the Debye–Callaway model. (e) and (f) SEM images for the samples with $x = 0.02$ and 0.04, respectively.

The lattice thermal conductivity κ_l as a function of x at room temperature is displayed in Fig. 3(d). We analyzed the variation of κ_l on the basis of the Debye–Callaway model.[18] At the beginning, κ_l increases for $x = 0.01$ owing to the decrease of Sn vacancies. Amazingly, κ_l decreases rapidly for $x = 0.02$ and deviates from the theoretical model, while κ_l increases again for $x = 0.04$ falling on the vicinity of the prediction, indicating an extra mechanism of phonon scattering. To explore the inherent origin, we carried out the SEM analysis for $x = 0.02$ and 0.04, as shown in Figs. 3(e) and 3(f). Dense precipitates embedded in the matrix are observed, which is responsible for the distinct decline of κ_l from ~ 1.7 $W\cdot m^{-1}\cdot K^{-1}$ ($x = 0$) to ~ 0.8 $W\cdot m^{-1}\cdot K^{-1}$ ($x = 0.02$) due to the strong phonon scattering. We have also checked statistical analysis

for the size distribution of precipitates. For $x = 0.02$, majority sizes of precipitates are less than 200 nm, while for $x = 0.04$, most sizes of precipitates are located in the range from 200 mm to 300 nm. The relative smaller size of precipitates cause the stronger phonon scattering, resulting in lower κ_l of $x = 0.02$ than that of $x = 0.04$.

Finally, the thermoelectric performance is evaluated by the dimensionless figure of merit $zT = S^2\sigma T/\kappa$, as shown in Fig. 4(a). The values of zT promptly increase with increasing the temperature. Particularly, for Zn-doped samples, the values of zT are substantially improved. The value of zT at 775 K for the pristine sample is ~ 0.2; it is improved by 100% to be ~ 0.5 for $x = 0.02$. Figure 4(b) summarizes the schematic band diagram and mechanism of phonon scattering, illuminating the enhancement of thermoelectric performance. In addition, the decreased band offset $\Delta E_{L-\Sigma}$ and increased band gap E_g due to Zn-doping play important roles in the improvement of Seebeck coefficient S power factor PF. Moreover, the precipitates embedded in the matrix contribute to the reduction of lattice thermal conductivity κ_l through additional phonon scattering.

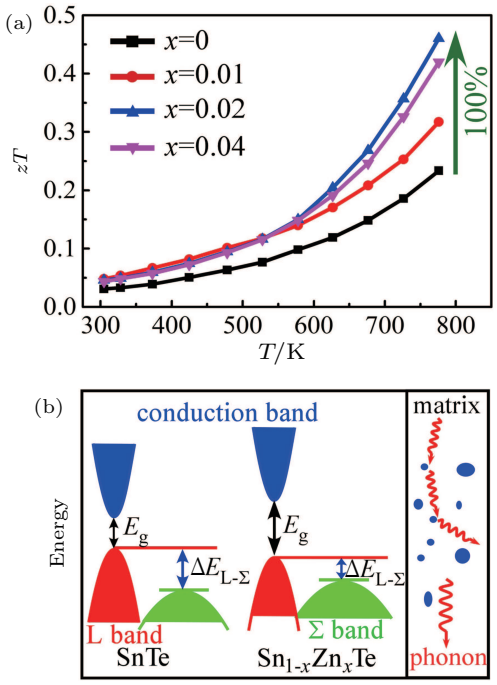


Fig. 4. (color online) (a) Temperature-dependent dimensionless figure of merit zT for all samples. (b) Schematic diagram of band structure and schematic illustration of phonon scattering by precipitates embedded in a matrix derived from SEM images.

4. Conclusion

We have demonstrated the large enhancement of thermoelectric performance in SnTe by Zn-doping, which arises from the band engineering and embedded precipitates. The carrier concentration n and effective mass m^* manipulate Seebeck coefficient S and power factor PF through Zn-doping. The strengthened phonon scattering by precipitates leads to the decrease of lattice thermal conductivity κ_l. The band gap widening suppresses the bipolar effect. The improved performance makes Zn-doped SnTe a promising candidate for thermoelectric applications.

Acknowledgment

The authors thank Prof. Yanzhong Pei from Tongji University for his support and discussion on Hall measurement.

References

[1] LaLonde A D, Pei Y and Snyder G J 2011 *Energy Environ. Sci.* **4** 2090
[2] Snyder G J and Toberer E S 2008 *Nat. Mater.* **7** 105
[3] Kleinke H 2010 *Chem. Mater.* **22** 604
[4] Nolas G S, Cohn J L, Slack G A and Schujman S B 1998 *Appl. Phys. Lett.* **73** 178
[5] Toberer E S, May A F and Snyder G J 2010 *Chem. Mater.* **22** 624
[6] Kauzlarich S M, Brown S R and Snyder G J 2007 *Dalton Trans.* **0** 2099
[7] Makongo J P, Misra D K, Zhou X, Pant A, Shabetai M R, Su X, Uher C, Stokes K L and Poudeu P F 2011 *J. Am. Chem. Soc.* **133** 18843
[8] Fu C, Bai S, Liu Y, Tang Y, Chen L, Zhao X and Zhu T 2015 *Nat. Commun.* **6** 8144
[9] Sales B C, Mandrus D and Williams R K 1996 *Science* **272** 1325
[10] Ren W, Geng H, Zhang Z and Zhang L 2017 *Phys. Rev. Lett.* **118** 245901
[11] Wu H J, Zhao L D, Zheng F S, Wu D, Pei Y L, Tong X, Kanatzidis M G and He J Q 2014 *Nat. Commun.* **5** 4515
[12] Wei T R, Tan G, Wu C F, Chang C, Zhao L D, Li J F, Snyder G J and Kanatzidis M G 2017 *Appl. Phys. Lett.* **110** 053901
[13] Cao B L, Jian J K, Ge B H, Li S M, Wang H, Liu J and Zhao H Z 2017 *Chin. Phys. B* **26** 017202
[14] Li W, Wu Y, Lin S, Chen Z, Li J, Zhang X, Zheng L and Pei Y 2017 *ACS Energy Lett.* **2** 2349
[15] Wang L J, Chang S Y, Zheng S Q, Fang T, Cui W L, Bai P P, Yue L and Chen Z G 2017 *ACS Appl. Mater. Interfaces* **9** 22612
[16] Li Z, Chen Y, Li J, Chen H, Wang L, Zheng S, Wang L, Zheng S and Lu G 2016 *Nano Energy* **28** 78
[17] Rogers L M 1968 *J. Phys. D: Appl. Phys.* **1** 845
[18] Pei Y, Zheng L, Li W, Lin S, Chen Z, Wang Y, Xu X, Yu H, Chen Y and Ge B 2016 *Adv. Electron. Mater.* **2** 1600019
[19] Li W, Zheng L, Ge B, Lin S, Zhang X, Chen Z, Chang Y and Pei Y 2017 *Adv. Mater.* **29** 1605887
[20] Zhou M, Gibbs Z M, Wang H, Han Y, Li L and Snyder G J 2016 *Appl. Phys. Lett.* **109** 042102
[21] Tan G, Zhao L D, Shi F, Doak J W, Lo S H, Sun H, Wolverton C, Dravid V P, Uher C and Kanatzidis M G 2014 *J. Am. Chem. Soc.* **136** 7006
[22] Banik A, Shenoy U S, Anand S, Waghmare U V and Biswas K 2015 *Chem. Mater.* **27** 581
[23] Li W, Chen Z, Lin S, Chang Y, Ge B, Chen Y and Pei Y 2015 *J. Materiomics* **1** 307
[24] Wu H, Chang C, Feng D, Xiao Y, Zhang X, Pei Y, Zheng L, Wu D, Gong S, Chen Y, He J, Kanatzidis M G and Zhao L D 2015 *Energy Environ. Sci.* **8** 3298
[25] Zhang Q, Liao B, Lan Y, Lukas K, Liu W, Esfarjani K, Opeil C, Broido D, Chen G and Ren Z 2013 *Proc. Natl. Acad. Sci. USA* **110** 13261
[26] Tan G, Shi F, Doak J W, Sun H, Zhao L D, Wang P, Uher C, Wolverton C, Dravid V P and Kanatzidis M G 2015 *Energy Environ. Sci.* **8** 267
[27] Dong X, Yu H, Li W, Pei Y and Chen Y 2016 *J. Materiomics* **2** 158
[28] Nasirov Y N, Sultanova N P and Osmanov T G 1969 *Phys. Stat. Sol.* **35** K39
[29] Pei Y, Shi X, LaLonde A, Wang H, Chen L and Snyder G J 2011 *Nature* **473** 66
[30] Zhou M, Gibbs Z M, Wang H, Han Y M, Xin C N, Li L F and Snyder G J 2014 *Phys. Chem. Chem. Phys.* **16** 20741
[31] Vedeneev V P, Krivoruchko S P and Sabo E P 1998 *Semiconductors* **32** 241